Process-level constraints on aerosol-cloud interactions in convective anvils

Maor Sela*, Mathilde Ritman, Sadhitro De, Philip Stier
Atmospheric, Oceanic, and Planetary Physics, Department of Physics, University of Oxford

EUROPEAN SPACE AGENCY

Background

Anthropogenic aerosols acting as CCN are known to impact warm cloud processes, but their influence on deep convective clouds (DCCs) and ice microphysics is poorly constrained. Suppression of warm rain processes leads to transport of smaller, more numerous supercooled droplets above the melting layer, modifying the relative importance of riming and vapour deposition as ice growth pathways. Here we show that this shift in ice growth mechanism propagates to the anvil, with consequences for anvil cloud radiative effect.

Experiment:

Houston, TX. sea-breeze case[1] (June 17, 2022), using the *tobac*[2] cloud-tracking algorithm, with three runs: baseline, X3, and X0.3 the aerosol concentrations and emissions.

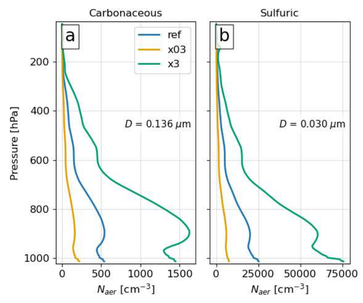

Fig. 1. Domain mean of the vertical profile of (a) the carbonaceous and (b) sulfuric modes in ICON-HAMlite[3], with the baseline (ref) in blue, polluted (X3) in green, and clean (X0.3) in orange.

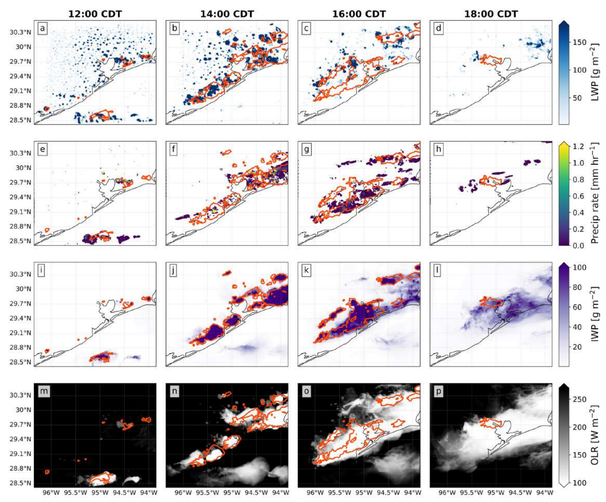

Fig. 2. Instantaneous maps of (a) LWP, (b) surface precipitation, (c) IWP, and (d) OLR during the span of the convective storm on June 17, 2022, as simulated by the reference run. Tracked cells contours are overlaid in red.

Convective response

The aerosol concentrations impact the domain mean precipitation, cloud profile, and cloud droplet and ice crystal number concentrations, where the most polluted case shows delayed and diminished precipitation, more numerous droplets and crystals. In addition, the aerosol perturbations impact cloud morphology, with larger ice and snow, but smaller hail extent in the most polluted case.

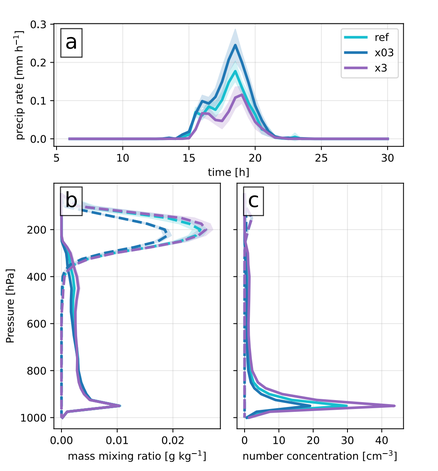

Fig. 3. Domain mean of (a) surface precipitation, (b) cloud water (solid) and ice (dashed) mass mixing ratio, and (c) cloud droplet (solid) and ice crystal (dashed) number concentration for the reference (light blue), clean (blue), and polluted (purple) cases. Shading shows ensemble standard deviation.

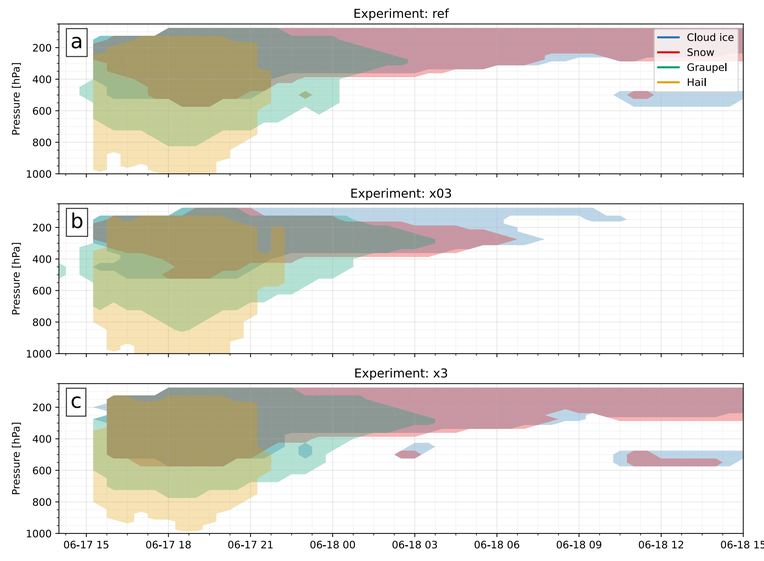

Fig. 4. Pressure-time evolution of the ice habits distribution for the (a) reference, (b) clean, and (c) polluted cases. Filled contours indicate regions where the mixing ratio of cloud ice (blue), snow (red), graupel (green), and hail (yellow) exceeds 0.1 mg kg^{-1}, averaged across members.

Microphysics competition

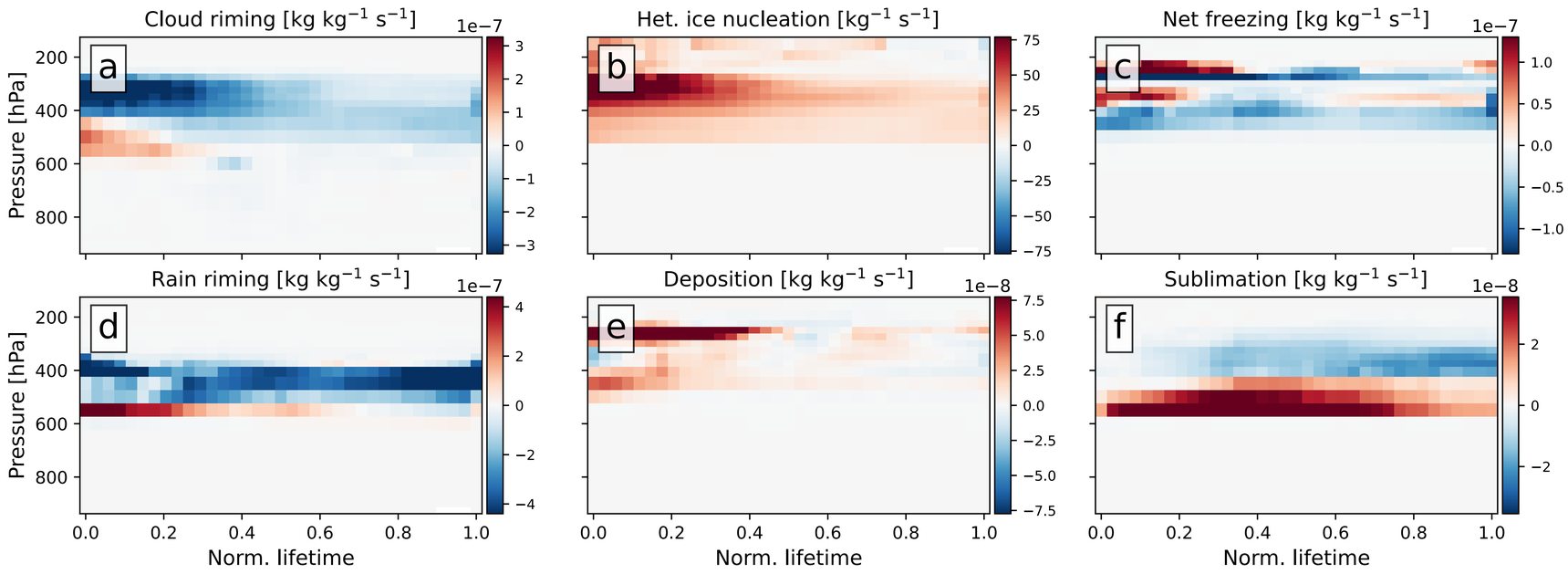

Fig. 5. Differences in ice-phase process rates (x3 − x0.3): (a) cloud riming, (b) ice nucleation, (c) net freezing, (d) rain riming, (e) vapour deposition, and (f) sublimation, as a function of the normalised tracked system lifetime and pressure, averaged across the ensemble. The Lagrangian tracking identifies coherent 3D convective objects, ensuring all signals belong to the tracked DCC. Red (blue) indicates enhanced (suppressed) rates in the polluted relative to the clean experiment. Note that colorbar scales differ by an order of magnitude between riming (a, d) and deposition/sublimation (e, f).

Process rates show the tension between anvil sinks (riming and sublimation) and sources (ice nucleation and vapour deposition), with the polluted case showing reduced riming of cloud droplets and rain, and enhanced ice nucleation and vapour deposition above the melting layer, shifting ice growth from riming-dominated to deposition-dominated. In addition, the polluted case shows enhanced sublimation in the mixed-phase region but reduced sublimation in the anvil, with more net freezing early in the anvil lifecycle, consistent with longer crystal residence times.

CRE consequence

The differences in the system morphology and process rate translate to a consistent cloud radiative effect (CRE) in both shortwave and longwave: the most polluted case shows enhanced LW warming (larger spatial and temporal extent) and SW cooling (higher optical depth), with a net aerosol effect of 4.5 W m^{-2}.

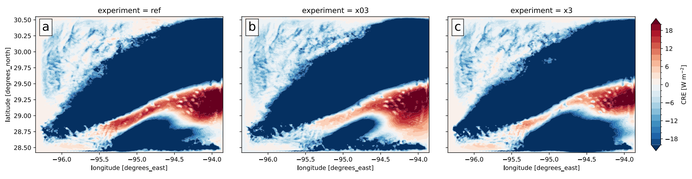

Fig. 6. Time-averaged total CRE maps, depicted from the entire domain, during the entire experiment duration (24 h), for the (a) reference, (b) clean, and (c) polluted cases.

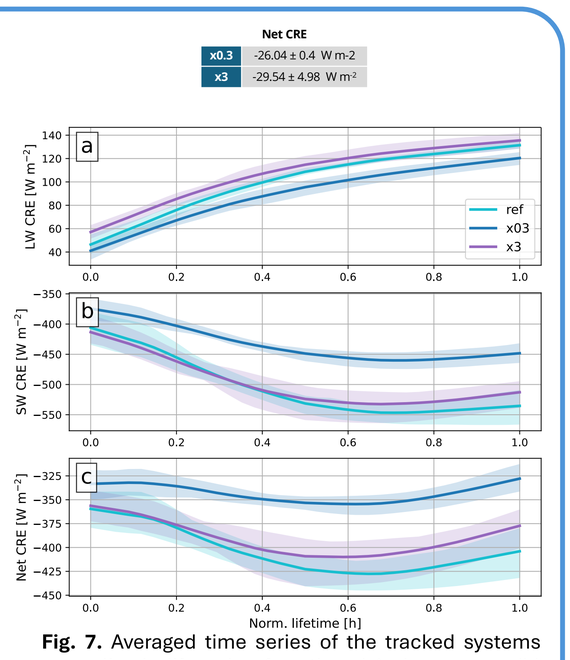

Fig. 7. Averaged time series of the tracked systems normalised lifecycle for the (a) longwave, (b) shortwave, and (c) total CRE for the reference (light blue), clean (blue), and polluted (purple) cases.

Observational constraint

This process-level framework identifies the microphysical fingerprint of aerosol perturbations in DCC anvils, but the simulated shift from riming- to deposition-dominated ice growth remains observationally unconstrained. Constraining it requires vertical profiles of ice crystal habit, fall speed, and size distribution across the DCC lifecycle. Radar and Doppler velocity measurements (from TRACER/EarthCARE) offer a direct path toward testing whether this aerosol-driven microphysical transition is detectable in real convective systems.

→ Can we observe the riming-to-deposition shift across the DCC anvil lifecycle?

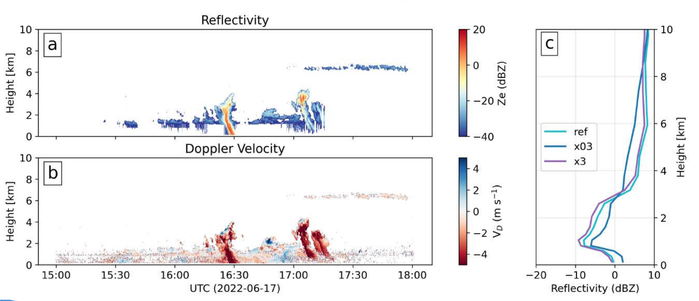

Fig. 8. Height-time curtains of (a) radar reflectivity and (b) Doppler velocity from the TRACER's Ka-Band ARM Zenith Radar (KAZR)[4] at La Porte, TX, on June 17, 2022. No DCC overpass was recorded above the station during this period. Panel (c) shows mean reflectivity profiles from the Cloud-Resolving Model Radar Simulator (CR-SIM) for the reference (light blue), clean (blue), and polluted (purple) simulations, illustrating the simulated observational signatures that future collocated observations could constrain.

Acknowledgments

The simulations were performed and analysed on the Levante cluster of the DKRZ with resources granted under project 1368 (https://www.dkrz.de/en/systems/hpc/hlre-4-levante). We also acknowledge funding from the NERC DTP in Environmental Research Grant NE/S007474/1, and the European Union's Horizon Europe project CleanCloud with grant agreement 101137639 and its UKRI underwrite. TRACER data were obtained from the Atmospheric Radiation Measurement (ARM) Program sponsored by the U.S. Department of Energy, Office of Science, Office of Biological and Environmental Research, Climate and Environmental Sciences Division.

References

1. Jensen M. P., J. H. Flynn III, P. Kollias, C. Kuang, et al. 2023. Tracking Aerosol Convection Interactions Experiment (TRACER) Field Campaign Report. Ed. by Robert Stafford, ARM user facility. DOE/SC ARM-23-038. https://doi.org/10.2172/2202672.
2. Ritman, M., Jones, W., and Stier, P.: Convective controls on anvil cloud evolution in the ICON km-scale global climate model, Atmos. Chem. Phys., 26, 7105–7126, https://doi.org/10.5194/acp-26-7105-2026, 2026.
3. Weiss, P., Herbert, R., and Stier, P.: ICON-HAM-lite 1.0: simulating the Earth system with interactive aerosols at kilometer scales, Geosci. Model Dev., 18, 3877–3894, https://doi.org/10.5194/gmd-18-3877-2025, 2025.
4. Atmospheric Radiation Measurement (ARM) user facility. 2021. Ka ARM Zenith Radar (KAZRCFRGE), 2022-06-17 to 2022-06-18, ARM Mobile Facility (HOU) Houston, TX; AMF1 (main site for TRACER) (M1). Compiled by I. Lindenmaier, K. Johnson, D. Nelson, A. Matthews, T. Wendler, V. Melo de Castro, M. Deng, M. Rocque and Y. Feng. ARM Data Center. Data set accessed 2025-11-04 at http://dx.doi.org/10.5439/1498936.

EarthCARE 2026 Science and Validation workshop

8–12 June 2026 | Rhodes House | Oxford, UK

*maor.sela@physics.ox.ac.uk